Materials Science in Semiconductor Processing 122 (2021) 105474

Contents lists available at ScienceDirect

Materials Science in Semiconductor Processing

journal homepage: http://www.elsevier.com/locate/mssp

Nanostructure, optical and electrical response of gamma ray radiated PdS/p-Si heterojunction

Syed Mansoor Ali [a,*], M.S. AlGarawi [a], Salah Ud-Din Khan [b], S. Aldawood [a,**]

[a] Department of Physics and Astronomy, College of Science, P.O. BOX 2455, King Saud University, Riyadh, 11451, Saudi Arabia

[b] Sustainable Energy Technologies Center, College of Engineering, P.O. BOX 800, King Saud University, Riyadh, 11451, Saudi Arabia

ARTICLE INFO

Keywords:
Gamma ray exposure
I–V characteristics
SILAR
PdS/p-Si heterojunction
Photoluminescence

ABSTRACT

The palladium sulfide/p-type Si (PdS/p-Si) heterojunction was used to investigate the effects of gamma ray exposure on the structural, optical and current-voltage (I–V) characteristics, for gamma detection. High-quality PdS thin films was deposited onto p-Si substrates and evaluated as active components of the heterojunction. The PdS thin films was prepared using a successive ionic layer adsorption and reaction (SILAR) technique. The samples were then irradiated using a^{60}Co gamma source at dose of up to 100 kGy. X-ray diffraction (XRD) analysis indicated the formation of a tetragonal phase in the PdS thin films, an increase in crystallinity and a decrease in the crystallite size. The distributions of spherical grains on the surfaces of the substrate were observed using a field emission scanning electron microscope (FE-SEM) and energy dispersive X-ray (EDX) analysis was performed to determine the stoichiometric compositions of the PdS thin films. The FE-SEM images revealed the presence of voids after irradiation. Photoluminescence (PL) spectroscopy indicated an increase in the recombination rate of electron-hole pairs after irradiation, and spectral broadening occurred as a function of the gamma dose. The I–V characteristics of the PdS/p-Si heterojunction were investigated before and after irradiation. Changes in the electrical properties of the heterojunctions induced by irradiation, including the saturation current, ideality factor, barrier height, series resistance and shunt resistance, were investigated. The linear electrical responses of the PdS/p-Si heterojunction indicated that they were highly sensitive to gamma radiation. The outstanding electrical and optical responses of the PdS/p-Si heterojunction in accordance with the gamma dose indicated that they could be used for radiation dosimetry.

1. Introduction

Transition metal sulfides have electrical, optical, magnetic, and structural properties [1] that are important for a variety of advanced technical applications. These include infrared (IR) detectors, photoconductors [2], solar cells [3], gas sensors [4], fuel cells [5], light-emitting diodes [6], lithium ion batteries [7] and spintronics [6]. As compared to the other the transition metal sulfides (CdS, PbS, CuS, ZnS), palladium sulfide (PdS) is one of the least studied. Palladium sulfide structural phases are diverse and include PdS, Pd_3S, Pd_4S, PdS_2, $Pd_{25}S$, $Pd_{22}S$ and $Pd_{28}S$. Vysotskite PdS which has a band gap of ~2 eV is the most common among them. It is highly conductive [8] with semiconducting properties that makes it a potential candidate for advanced applications and devices. These include photocatalysis [9], high-temperature electrodes [10], semiconducting electronic devices [11], acid-resistant films and lithographic films [12].

Several PdS deposition techniques have been developed, which include solvothermal routes, chemical vapor deposition (CVD), non-CVD methods, photochemical CVD, thermal deposition, AACVD and low pressure MOCVD [13–19]. In this work, PdS thin films were deposited using a successive ionic layer adsorption and reaction (SILAR) method. The SILAR technique has the advantages of low cost and simplicity. Deposition can be performed over a large area at room temperature and ambient pressure and the thickness of the film can be controlled [20].

Exposure to gamma rays generates a wide variety of defect states in a host material which is due to the transfer of large amounts of energy. Changes in the electron configuration alter the electrical properties of the material and consequently its structural and optical properties [21, 22]. The induced deviations depend on the gamma ray dose. These

* Corresponding author.
** Corresponding author.
E-mail addresses: Symali@ksu.edu.sa (S.M. Ali), sdawood@ksu.edu.sa (S. Aldawood).

https://doi.org/10.1016/j.mssp.2020.105474
Received 22 March 2020; Received in revised form 24 August 2020; Accepted 23 September 2020
Available online 5 October 2020
1369-8001/

defects generally act as recombination centers that reduce the diffusion lengths and lifetimes of charge carriers, which leads to changes in the properties of the heterojunction. The electrical parameters of the heterojunction, such as the saturation current, ideality factor, barrier height, series resistance and shunt resistance, also depend on the gamma ray dose. Energetic photons transfer energy in the material lattice following gamma ray exposure. This can either produce defect states or remove existing defects, which can change the defect density within the material. These variations could potentially change the electronic, nanostructural and optical characteristics of PdS/p-Si heterostructure [23]. To the best of our best knowledge, the effects of gamma ray exposure on the properties of PdS/p-Si heterojunctions have not been thoroughly investigated. There have been a few studies on the effects of gamma rays on the nanostructural, optical, and electronic properties of p-n heterojunction. For example, Laranjeira et al. reported that the optical characteristics of polyaniline (PANI) were strongly affected by interactions with gamma radiation in a study on polyaniline/silicon heterojunction for gamma radiation detection [24]. Balboul et al. studied alterations in the direct current (DC) electrical conductivity and activation energy of CdS thin films due to gamma ray exposure [25]. Zhang et al. reported on the effects of ^{60}Co gamma irradiation on the DC and AC characteristics of a InGaP/GaAs single heterojunction [26].

In this work, we investigated the dose-dependent effects of gamma rays on the properties of PdS/p-Si heterojunction. To fabricate the PdS/p-Si heterojunction PdS thin films was deposited onto p-Si substrates using the successive ionic layer adsorption and reaction (SILAR) technique. The prepared samples were irradiated using a ^{60}Co gamma source. The crystalline properties, surface morphology, stoichiometry, diffuse reflectance, energy band gap and I–V characteristics of each sample were evaluated before and after gamma irradiation. The dose-dependent responses of the PdS/p-Si heterojunction were also examined to evaluate the feasibility of using this material for radiation dosimetry applications.

2. Methods and techniques

To fabricate the PdS/p-Si heterojunction, thin films were first prepared on p-type Si substrates using palladium nitrate ($Pd(NO_3)_2$) and sodium sulfide (Na_2S) via the SILAR method. To remove the oxide layer, the Si substrate was dipped in 35% HCl for 10 min at room temperature and washed with deionized water prior to thin-film deposition. We prepared a 0.5 M solution of $Pd(NO_3)_2$ in water and added a few drops of triethanolamine (TEA) to serve as a Pd^{2+} source. A 0.5 M solution of Na_2S in ethanol was prepared to provide S^{2-}. The Si substrates were first dipped in the cation solution for 30 s to allow the Pd^{2+} to adsorb. The substrates were rinsed with deionized water to eliminate the excess Pd^{2+}, then immersed in the anion solution for 30 s. The S^{2-} was allowed to react with the adsorbed Pd^{2+} and the surfaces were rinsed with ethanol to remove loosely bound ions. The entire process comprised one SILAR cycle for PdS thin-film deposition. Fifteen SILAR cycles were performed to obtain PdS thin films with the desired thicknesses.

The prepared PdS/p-Si heterojunctions were irradiated using a 1.25 MeV gamma cell 220 Excel irradiator (MDS Nordion). The activity of the ^{60}Co gamma source was 7.328 kGy/h, and the heterojunctions were subjected to doses of 25, 50, and 100 kGy. After gamma ray exposure, 50 nm thick Pt electrodes were deposited over an area of $\sim 2.5 \times 10^{-5}$ m^2 at the top and bottom using a sputter coater.

The PdS/p-Si heterojunctions were structurally characterized before and after irradiation. X-ray diffraction (XRD) analysis was performed using a Panalytical X'Pert^3 MRD diffractometer (Malvern Panalytical) equipped with a CuKα radiation source. The morphology of the films was examined using a field emission scanning electron microscope (FE-SEM, JEOL). Optical characterization was performed using a V-670 UV–visible spectrophotometer (JASCO) and a FP-8200 spectrofluorometer (JESCO). The electrical properties were investigated using a 4200 semiconductor characterization system (Keithley).

3. Results and discussion

The XRD patterns of the PdS/p-Si heterojunctions before and after gamma irradiation are shown in Fig. 1 (a). The results confirmed the crystalline nature of the PdS thin films. The intensity and full width at half-maximum (FWHM) in the preferred direction increased as the gamma dose increased, which was consistent with increasing crystallinity and decreasing crystallite size. The XRD peaks were indexed to JCPDS card no. 78–0206 and confirmed the presence of a Vysotskite crystal structure in the tetragonal phase ($P4_2/m$). The lattice constants were 6.28 Å (a) and 6.69 Å (c), which were in good agreement with previously reported values [27–29]. The XRD patterns did not indicate the presence of impure phases, such as $Pd_{28}S$, PdO, Pd_3S, Pd_4S, $Pd_{22}S$, and $Pd_{25}S$.

Peak broadening is related to crystallite size and micro-strain, which arises from crystal deficiencies and distortion [30]. The relationship between the peak positions, crystallite size (D) and micro-strain (ε) was investigated by creating Williamson-Hall (W–H) plots based on Equation (1) [31].

$$\beta \cos \theta = \frac{\lambda}{D} + 4\varepsilon \sin \theta, \tag{1}$$

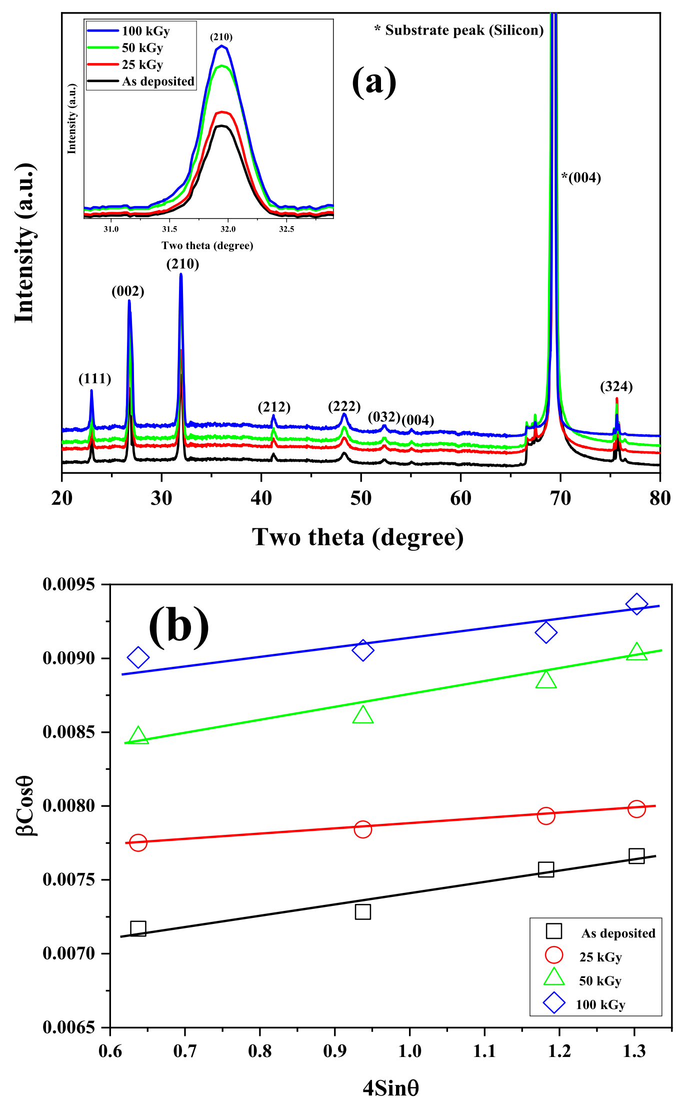

Fig. 1. (a) XRD patterns of as-deposited and gamma-irradiated PdS/p-Si heterojunctions. The (210) peaks of the samples are enlarged in the inset. (b) Williamson-Hall plots of the samples.

where β is the FWHM of the peak. D and ε were determined by plotting βcosθ against 4sinθ for the indexed peaks of PdS thin films containing the tetragonal phase. The slope and y-intercept of the fitted line represent micro-strain and crystallite size, respectively. The W–H plots of the as-prepared and irradiated samples are shown in Fig. 1 (b) and the calculated values are summarized in Table 1. The results indicated that micro-strain and crystallite size in the irradiated samples decreased as the gamma dose increased. This is due to the lattice mismatch with the Si substrate or structural defects caused by irradiation, such as dislocations [32].

FE-SEM images revealing the surface morphologies of the PdS/p-Si heterojunctions before and after irradiation are shown in Fig. 2(a–d). The spherical PdS grains were randomly distributed on the surfaces of the Si substrates. Voids that were present prior to gamma ray exposure were larger after irradiation and their sizes increased with dosage. Nano-grains on the irradiated surfaces were agglomerated with a ginger-like morphology. This may have been due to the large surface area of the nano-grains. They absorbed more energy as the gamma dose increased which resulted in agglomeration and the formation of clusters [33]. With increasing dosage the surfaces grew increasingly non-uniform and the thin films become rough. The average grain size decreased from ~54 nm to ~34 nm as the dosage increased from 0 kGy to 100 kGy. A cross-sectional view of a PdS/p-Si heterojunction is shown in Fig. 2 (e). The deposited PdS thin film on the Si substrate had a dense and crystalline structure with a thickness of ~165 nm. The Pt electrode and the PdS thin film could be clearly distinguished which indicated good contact with the Si substrate.

The EDX spectrum of an as-prepared PdS/p-Si heterojunction is shown in Fig. 3. The spectrum confirmed the presence of Pd, S and Si in the prepared sample. The elemental composition of the as-prepared sample is shown in the inset.

Diffuse reflectance (DR) spectroscopy was performed to investigate the optical behavior of the as-prepared and irradiated PdS/p-Si heterojunctions. The spectra of the as-prepared and irradiated heterojunctions from 600 nm to 850 nm were recorded at room temperature. The spectra are shown in Fig. 4 (a). PdS absorbed strongly at wavelengths between 600 nm and 675 nm with a band edge at 729 nm. A red shift was observed as the gamma ray dose increased. The DR spectra indicated that the reflectance of the PdS thin films in the visible region was lower following gamma ray exposure, which may have been due to a decrease in the roughness of the thin films. The most important feature of the DR spectroscopy data was that it allowed us to precisely determine the energy band gaps of the thin films.

The energy band gap value of the PdS thin films with non-irradiated and irradiated PdS/p-Si heterojunctions were determined by applying the Kubelka-Munk function based on Equation (2) [34,35].

$$F(R) = \frac{(1-R)^2}{2R}, \tag{2}$$

where R is the DR value. $F(R)$ is the Kubelka-Munk function, which is related to the absorption coefficient (α). The absorption coefficient was calculated using Equation (3).

$$\alpha = \frac{F(R)}{t}, \tag{3}$$

Table 1
Nanostructural and optical parameters as-deposited and irradiated PdS/p-Si heterojunctions.

Gamma dose (kGy)	Crystallite size (D, nm)	Micro-strain (ε, 10^{-3})	Energy band gap (eV)
0	44.60	11.34	1.47
25	38.55	10.19	1.49
50	33.49	9.96	1.56
100	26.14	8.81	1.59

where t is the thickness of the PdS thin film. The energy band gap was obtained using the Tauc's equation [36,37] as shown in Eq. (4).

$$(\alpha h\nu) = \frac{F(R)h\nu}{t} = A\left(h\nu - E_g\right)^n, \tag{4}$$

where A is a constant, E_g is the energy band gap, h is Planck's constant, ν is the frequency of the incident photon, and n is a constant that depends on the type of transition. For a direct allowed transition, $n = 1/2$. The deviation of $(\alpha h\nu)^2$ is shown as a function of $h\nu$ in the Tauc plots in Fig. 4 (b). The linear regions of the plots were extrapolated to the x-axes to determine the energy band gaps of the PdS/p-Si heterojunctions shown in Table 1. The band gap increased significantly with increasing gamma dosage. Increasing the gamma dosage reduced the mobility of free charge carriers in the PdS thin films which widened the band gap [38]. However, the influences of smaller crystallites and the presence of structural defects could not be ignored. An increase in the apparent band gap is referred to as the Burstein-Moss effect [39,40]. This is observed when states near the conduction band become more populated, and the Fermi level merges with the conduction band.

The photoluminescence properties of the PdS/p-Si heterojunctions were examined to investigate charge recombination and defects in the non-irradiated and irradiated samples. The photoluminescence (PL) spectra in Fig. 5 were collected at room temperature with excitation at 715 nm to gain insight into the recombination processes in the PdS/p-Si heterojunctions. The PL spectra of the as-prepared and irradiated samples contained a sharp emission band at 729.87 nm and a shoulder near 770 nm, which varied in intensity. The sharp band was attributed to the electron transition from the interstitial band of PdS to the valence band. The shoulder was ascribed to defects, which were associated with carrier trapping at the grain boundaries [41]. The notable broadening of the peak near 730 nm and the increase in excitation intensity with gamma dosage attributed in the pristine monolayer. The increase in intensity with increasing dosage was ascribed to spectral broadening and an increase in the recombination rate of electron-hole pairs [42]. Which may have been due to contributions from excitons trapped within the band gap.

Charge carrier transport and the electrical properties of the heterojunctions were analyzed by observing their current-voltage characteristics. We measured the current passing through each junction while applying a bias voltage. The I–V curves of the as-deposited and irradiated PdS/p-Si heterojunctions recorded in darkness at room temperature are shown inset of Fig. 6 (a). All of the samples exhibited nonlinear behavior, which suggested that fabrication of the PdS/p-Si heterojunctions was successful. The PdS/n-Si heterojunctions revealed a rectifying effect at ±4 V. The rectification ratio decreased from 30 to 15 as the gamma ray dose increased from 0 to 100 kGy. Several PdS/p-Si heterojunction parameters, including the saturation current, ideality factor, barrier height, and series resistance, were estimated from the I–V curves. The I–V properties of a heterojunction are defined according to Equation (5) [43].

$$I = I_s \exp\left(\frac{qV}{nkT}\right), \tag{5}$$

where q is the charge of an electron, V is the applied voltage, k is the Boltzmann constant and T is the absolute temperature. I_s the reverse saturation current, which is given by Equation (6) and the ideality factor (n) can be obtained using Equation (7) [44].

$$I_S = AA^* \exp\left(\frac{-q\varphi_b}{kT}\right) \tag{6}$$

and

$$n = \frac{q}{kT}\left(\frac{dV}{d(\ln I)}\right), \tag{7}$$

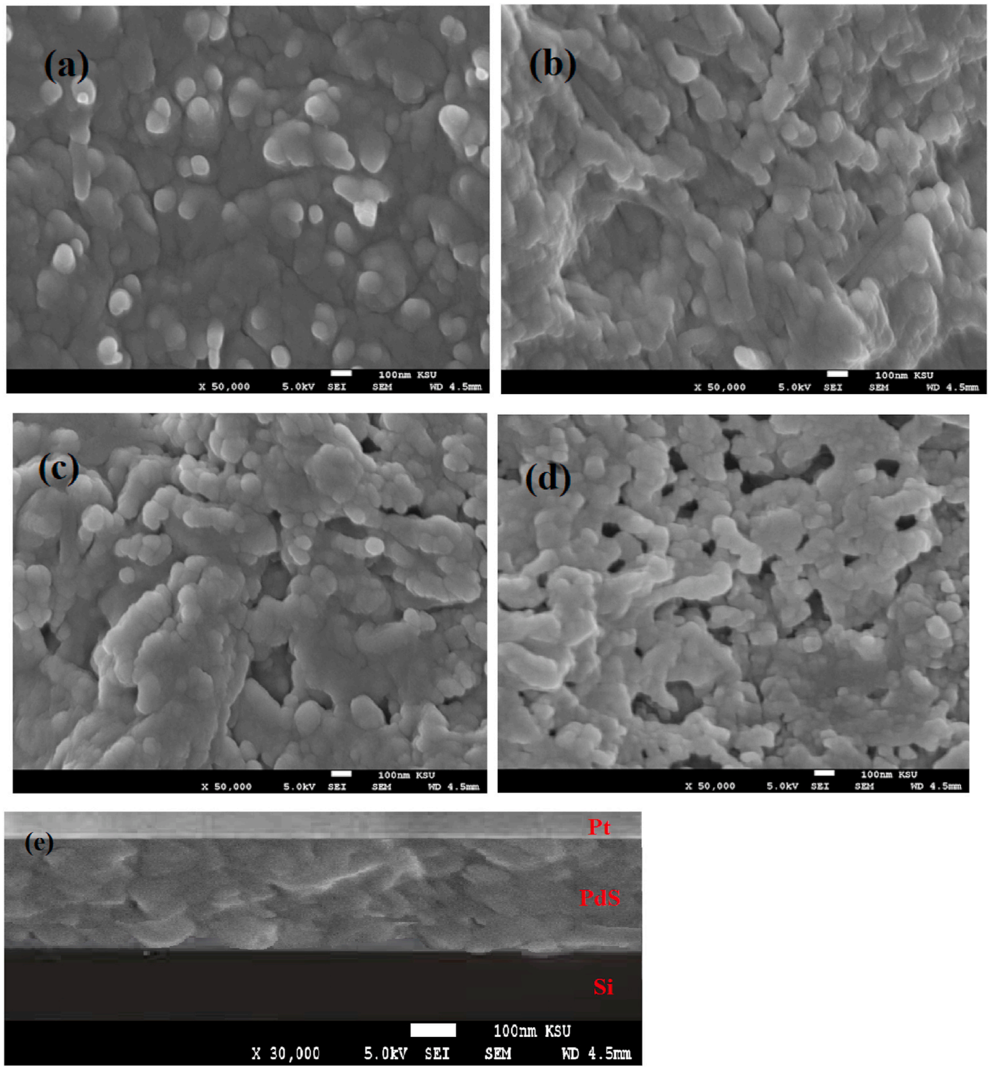

Fig. 2. FE-SEM images showing the morphologies of (a) an as-deposited sample and samples subjected to (b) 25 kGy, (c) 50 kGy, and (d) 100 kGy gamma irradiation. (e) Cross-sectional view of a PdS/p-Si heterojunction.

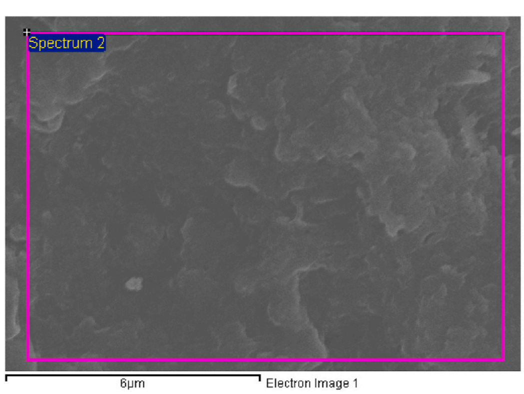

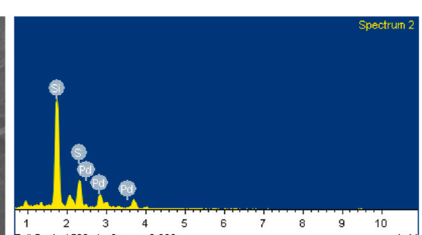

Element	Weight%	Atomic%
Si K	7.85	10.46
S K	70.05	81.76
Pd L	22.10	7.77
Totals	100.00	

Fig. 3. EDX spectrum and composition of an as-deposited PdS/p-Si heterojunction.

where A is the contact area and A^* is the Richardson constant (31.6 A/ cm^2 K^2) for p-type Si [39]. The values of n and I_s were calculated from the slopes and intercepts of the log (I) vs. V plots in Fig. 6(a). The barrier height (Φ_b) was estimated using Equation (8) [45].

$$\varphi_b = \frac{kT}{q}\ln\left(\frac{AA^*}{I_s}\right), \tag{8}$$

The n-values decreased as the gamma dosage increased. The PdS/p-Si heterojunctions had large values (>1) which may have been due to the recombination of electron-hole pairs in the depletion region [40]. The I_s decreased as the gamma ray dosage increased, while the value of Φ_b increased. This may have been due to the defect density or inhomogeneity of the interfacial layer [46]. The calculated heterojunction

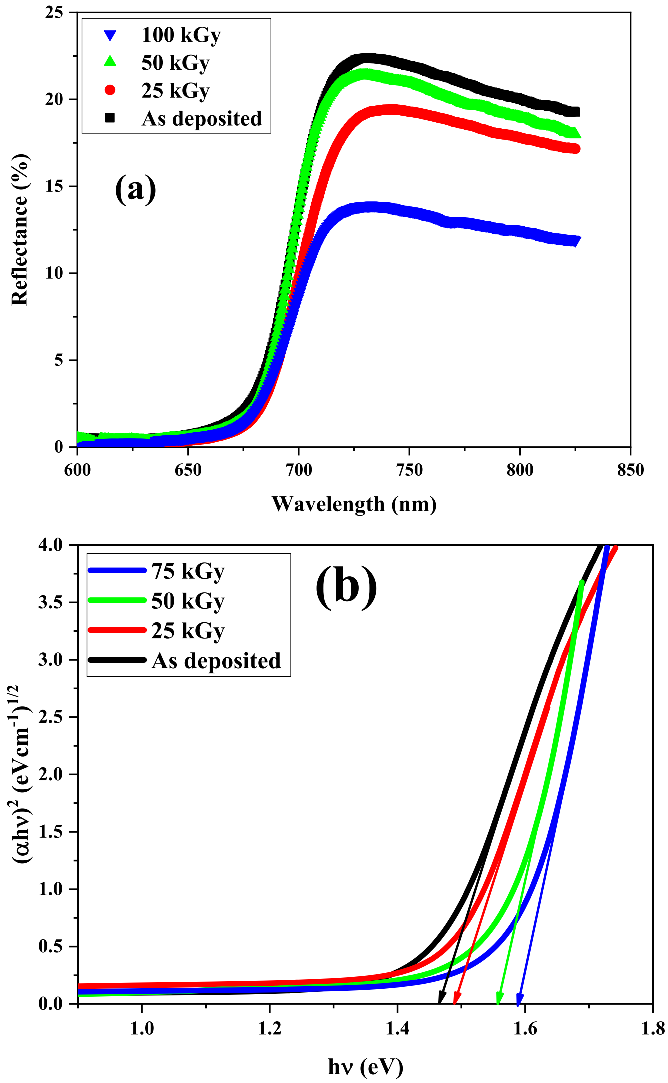

Fig. 4. (a) Diffuse reflectance spectra and (b) Tauc plots of the as -prepared and irradiated PdS/p-Si heterojunctions.

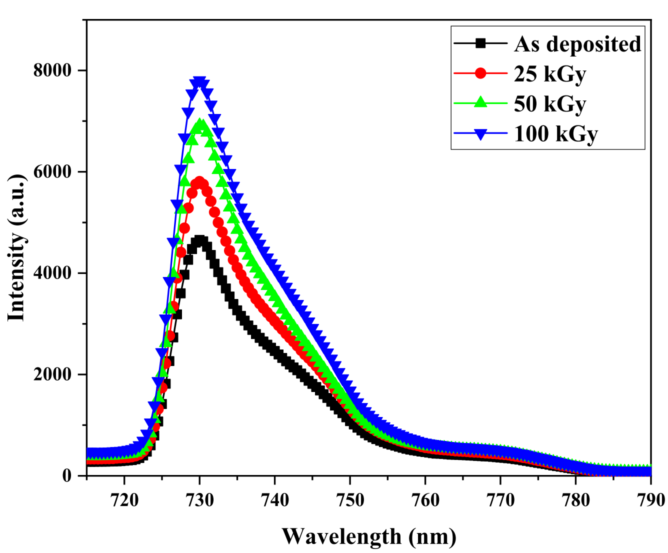

Fig. 5. PL spectra of as-deposited and irradiated PdS/p-Si heterojunctions.

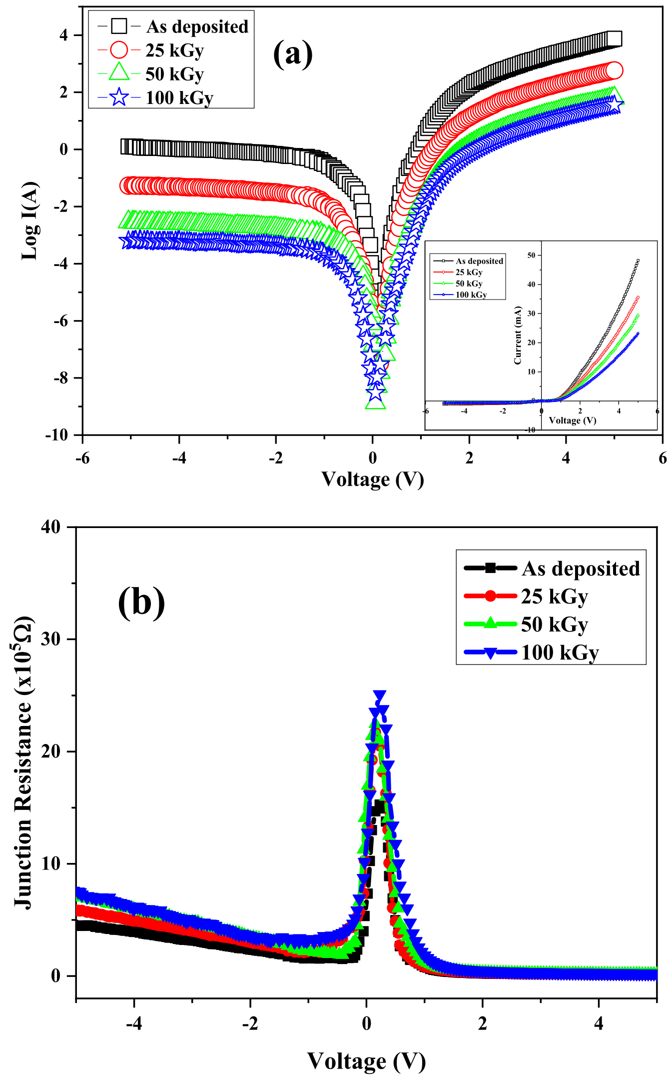

Fig. 6. I–V characteristics of the as-prepared and irradiated PdS/p-Si heterojunctions. (a) Log(I) vs. V and (b) junction resistance vs. applied voltage.

parameters are listed in Table 2.

The junction resistance (R_j) of each PdS/p-Si heterojunction was determined from the reciprocal slope of the I–V plot. The junction resistance of each heterojunction is plotted against the applied voltage in Fig. 6 (b). The series resistance (R_s) is the sum of the PdS thin-film resistance and the contact resistance in the heterojunction. The shunt resistance (R_{sh}) is due to the minor current flowing through the depleted region at the termini of the heterojunction. The R_s and R_{sh} values were determined from plots of R_j vs. V. With a large forward bias voltage R_j remained nearly constant and corresponded to R_s. When a large reverse bias was applied R_j approached R_{sh} [47]. The calculated R_s and R_{sh} values of the as-prepared and irradiated PdS/p-Si heterojunctions are shown in Table 2. R_s and R_{sh} increased as the gamma dose increased which may have been due to structural changes and interfacial inhomogeneities at the heterojunctions.

4. Conclusion

In this work the impact of gamma ray dosage on PdS/p-Si heterojunction was studied to evaluate the feasibility of using PdS for radiation dosimetry applications. PdS/p-Si heterojunctions were successfully fabricated by depositing PdS thin films onto p-Si substrates using a SILAR technique. The influence of gamma irradiation on the

Table 2
Electrical parameters of the as-prepared and irradiated PdS/p-Si heterojunctions.

Gamma Dose (kGy)	Ideality factor (*n*)		Saturation Current (A × 10^{-3})	Barrier Height (eV)	Series Resistance (kΩ)	Shunt resistance (kΩ)
	ln(I)–V	Cheung's method				
0	2.88	2.82	9.78	0.79	19	48
25	2.72	2.76	6.82	0.84	23	64
50	2.70	2.73	4.53	0.89	27	75
100	2.68	2.65	3.25	0.97	36	81

nanostructural, morphological, optical and I–V characteristics of PdS/p-Si were then examined. XRD analysis confirmed a Vysotskite crystal structure in the tetragonal phase. Crystallinity increased with increasing gamma ray dosage, while the crystallite size decreased. FE-SEM images showed dense spherical grains which had agglomerated into ginger-like structures after gamma ray exposure. EDX analysis confirmed the presence of Pd, S and Si in the prepared samples. The results of UV–visible spectroscopy indicated that increasing the gamma dosage reduced free charge carrier mobility in the PdS thin films, which increased the band gap from 1.47 to 1.59 eV. Sharp bands at 715 nm in the PL spectra of the samples were attributed to an electron transition from the interstitial band to the valence band of PdS. A shoulder was ascribed to defects associated with carrier trapping at the grain boundaries. Exposure of the PdS/p-Si heterojunctions to different gamma-dosages altered their forward and reverse I–V characteristics. These findings suggest that PdS/p-Si heterojunctions could be good candidates as radiation dosimetry materials.

Author statement

S. Aldawood and Syed Mansoor Ali designed the concept and conducted the experiments. Syed Mansoor Ali, S. Aldawood and Salah Ud-Din Khan, wrote the main manuscript and M. S. AlGarawi reviewed the paper.

Declaration of competing interest

The authors declare that they have no known competing financial interests or personal relationships that could have appeared to influence the work reported in this paper.

Acknowledgements

The authors extend their appreciation to the Deanship of Scientific Research at King Saud University for funding this work through research group No (RG- 1441-315).

References

[1] C.I. Pearce, R.A. Pattrick, D.J. Vaughan, Rev. Mineral. Geochem. 61 (2006) 127–180.
[2] Y. Chen, G.F. Huang, W.Q. Huang, B. Zou' A. Pan, Appl. Phys. Mater. Sci. Process 108 (2012) 895–900.
[3] X. Li, H. Shen, S. Li, J.Z. Niu, H. Wang, L.S. Li, J. Mater. Chem. 20 (2010) 923–928.
[4] H. Karami, S. Babaei, Int. J. Electrochem. Sci. (2013) 8.
[5] C.M. Grgicak, J.B. Giorgi, J. Phys. Chem. C 111 (2007) 15446–15455.
[6] C.H. Lai, M.Y. Lu, L.J. Chen, J. Mater. Chem. 22 (2012) 19–30.
[7] C.H. Lai, K.W. Huang, J.H. Cheng, C.Y. Lee, B.J. Hwang, L.J. Chen, J. Mater. Chem. 20 (2010) 6638–6645.
[8] J. Folmer, J. Turner, B. Parkinson, J. Solid State Chem. 68 (1987) 28.
[9] A. Mashkina, L. Sakhaltueva, Kinet. Catal. 43 (2002) 107–114.
[10] I. Ferrer, P.D. Chao, A. Pascual, C. Sanchez, Thin Solid Films 515 (2007) 5783–5786.
[11] K.E.K. Yamamoto, K. Endo, Y. Takaya, E. Kaneda, Mitsubishi Paper Mills Ltd., 1987. *Japanese Patent*, 62/226,155.
[12] P. Raybaud, J. Hafner, G. Kresse, H. Toulhoat, J. Phys. Condens. Matter 9 (1997) 11107.
[13] J. Grau, M. Akinc, J. Am. Ceram. Soc. 80 (1997) 941.
[14] G. Henshaw, I.P. Parkin, G.A. Shaw, J. Chem. Soc., Dalton Trans. (1997) 231.
[15] Q. Xuefeng, L. Yandong, X. Yi, Q. Yitai, Mater. Chem. Phys. 66 (2000) 97.
[16] M.A. Mansoor, M.A. Ehsan, V. McKee, N.-M. Huang, M. Ebadi, Z. Arifin, W. J. Basirun, M. Mazhar, J. Mater.Chem. A 1 (2013) 5284–5292.
[17] M.A. Mansoor, A. Ismail, R. Yahya, Z. Arifin, E.R. Tiekink, N.S. Weng, M. Mazhar, A.R. Esmaeili, Inorg. Chem. 52 (2013) 5624–5626.
[18] J. Cheon, D.S. Talaga, J.I. Zink, Chem. Mater. 9 (1997) 1208.
[19] M.A. Malik, P. O'Brien, N. Revaprasadu, J. Mater. Chem. 12 (2002) 92.
[20] S. Lindroos, M. Leskelä, Int. J. Inorg. Mater. 2 (2000) 197–201.
[21] A.M. Saad, A.K. Fedotov, A.V. Mazanik, Thin Solid Films 487 (2005) 202–204.
[22] M. Husham, Z. Hassan, M.A. Mahdi, A.M. Selman, N.M. Ahmed, Radiat. Phys. Chem. 92 (2013) 87–92.
[23] S. Karatasa, A. Turut, S. Altındal, Nucl. Instrum. Methods Phys. Res. B 555 (2005) 260.
[24] J.M.G. Laranjeira, H.J. Khoury, W.M. Azevedo, E.A. Vasconcelos, E.F. Silva, Protect. Dosim. 101 (2002) 85–88.
[25] M.R. Balboul, A. Abdel-Galil, I.S. Yahia, A. Sharaf, Adv. Mater. Sci. Eng. (2016) 3183909.
[26] Jincan Zhang, Kun Xu, Jinchan Wang, Min Liu, Liwen Zhang, Bo Liu, Qifeng Zhao, Radiation Effects & Defects in Solids, 2019, https://doi.org/10.1080/10420150.2019.1684916.
[27] F.S.F. Mahmoodi, P.T. Ahmad, M.F. Samavat, M.H. Tavakoli, S. Hadidchi, Open J. Phys. Chem. 2 (2012) 103–106.
[28] A.F. Khan, M. Mehmood, A.M. Rana, T. Muhammad, Appl. Surf. Sci. 256 (7) (2010) 2031–2037.
[29] P.A. Ajibade, A. Nqombolo, Chalcogenide Lett. 13 (2016) 427–434.
[30] M. Birkholz, Thin Film Analysis by X-ray Scattering, Wiley-VCH Verlag GmbH and Co. KGaA, Weinheim, 2006.
[31] A. Khorsand Zak, W.H.Abd Majid, M.E. Abrishami, Ramin Yousefi, Solid State Sci. 13 (2011) 251–256.
[32] R.C. Birtcher, L.M. Wang, Nucl. Instrum. Methods Phys. Res. B 59–60 (1991) 966–969.
[33] S.P. Ramnani, J. Biswal, S. Sabharwal, Radiat. Phys. Chem. 76 (2007) 1290–1294.
[34] P. Kubelka, F. Munk, Z Tech. Phys. 12 (1931) 593.
[35] P. Kubelka, J. Opt. Soc. Am. 38 (1948) 448.
[36] J. Tauc, A. Menth, J. Non-Cryst. Solids 569 (1972) 8–10.
[37] T. Kako, N. Kikugawa, J. Ye, Catal. Today 131 (2008) 197.
[38] S.M. Al-Sofiany, H.E. Hassan, J. Alloys Compd. 651 (2015) 149–156.
[39] B. Hapke, Theory of Reflectance and Emittance Spectroscopy, Cambridge University Press, Cambridge, UK, 2012.
[40] Y. Yang, C. Song, X. Wang, F. Zeng, F. Pan, J. Appl. Phys. 103 (2008), 074107.
[41] Y. Yang, J. Wu, X. Wang, Q. Guo, X. Liu, W. Sun, Y. Wei, Y. Huang, Z. Lan, M. Huang, J. Lin, H. Chen, Z. Wei, Adv. Mater. 32 (2020) 1904347.
[42] Y. Kanemitsu, T.J. Inagaki, M. Ando, Appl. Phys. Lett. 81 (2002) 141.
[43] S.M. Sze, Physics of Semiconductor Devices, second ed., Wiley, New York, 1981.
[44] A. Gumus, A. Turut, N. Yalcin, J. Appl. Phys. 91 (2002) 245.
[45] E.H. Rhoderick, Metal Semiconductor Contacts, Oxford University Press, Oxford, 1978.
[46] Z. Lin, Z. Yi-Men, Z. Yu-Ming, H. Chao, J. Semiconduct. 31 (2010) 114006.
[47] Sh A. Mansour, F. Yakuphanoglu, Solid State Sci. 14 (2012) 121–126.